

Supporting Information

Achieving Purely Organic Room Temperature Phosphorescence

Mediated by a Host-Guest Charge Transfer State

Weidong Qiu^a, Xinyi Cai^a, Mengke Li^a, Zijian Chen^a, Liangying Wang^a, Wentao Xie^a,
Kunkun Liu^{ab}, Ming Liu^{ac} and Shi-Jian Su^{*ab}

^a State Key Laboratory of Luminescent Materials and Devices and Institute of Polymer Optoelectronic Materials and Devices, South China University of Technology, Wushan Road 381, Tianhe District, Guangzhou 510640, Guangdong Province, P. R. China

E-mail: mssjsu@scut.edu.cn

^b South China Institute of Collaborative Innovation, Dongguan 523808, China

^c TCL China Star Optoelectronics Technology Co., Ltd., Shenzhen 518132, Guangdong Province, P. R. China

Table of Contents:

1. Experiment section
2. Detailed results
3. Calculation of the exciton dynamic rate constants
4. Materials
5. Reference

1. Experiments section

Chemical structure characterization. ^1H and ^{13}C NMR spectra were measured on a Bruker NMR spectrometer operating at 600 and 150 MHz, respectively. Atmosphere pressure chemical ionization (APCI) mass spectra were obtained using a JEOL JMS-K9 mass spectrometer. Powder XRD was conducted on a polycrystal X-ray diffraction (Rigaku SmartLab SE). Cyclic voltammetry (CV) measurement was conducted using the CHI-600D electrochemical workstation (with a glassy carbon electrode as working surface, a platinum wire as counter electrode and Ag/AgCl as reference electrode) scanning at the rate of 50 mV/s in nitrogen-saturated 0.1 mol/L n-Bu₄NPF₆ anhydrous solution. The HOMO energies were calculated from the oxidization peaks of cyclic voltammetry, while the LUMO energies were calculated according to the onset of absorption spectra in toluene and the HOMO energies. Electron spin-resonance spectroscopy was measured on a Bruker ELEXSYS-II E500 CW-EPR.

Sample preparation. Powder of guests and benzophenone (BP) were placed inside a glass vials with host-guest mass ratio of 99:1. The glass vials were transferred onto a hotplate which was heated to 70 °C. After the melting of BP and the guests were dissolved into the BP solution, the mixture was moved away from the heat source. And the liquid was dropped onto a quartz plate, forming a crystalline host-guest system.

Photophysical characterization. UV-vis absorption spectra were recorded using a Perkin-Elmer Lambda 950-PKA instrument. Solid state reflective UV-vis absorption spectra were measured by a Hamamatsu UV-3700 UV-VIS-NIR spectrophotometer. Fluorescence and phosphorescence spectra were recorded by a FluoroMax-4 spectrofluorometer. Transient PL decay spectra and temperature dependent PL spectra were conducted on a FL980 (Edinburgh Instrument) where the lifetimes in 50 μs time range were measured with a TCSPC laser and the lifetimes in ms and s time range were measured with a micro second flash lamp and Xeon lamp, respectively. For the pico-nanosecond lifetime measurements, a Ti Sapphire oscillator (80 MHz, Spectra physics) was used to be light source and an Optical Parameter (Inspire) was used to produce second harmonics excitation light. The lifetime was measured by a TCSPC (HydraHarp 400). Excitation intensity dependence PL intensity were measured using the same excitation source equipped with a spectra meter (Ocean Optics). Photoluminescent quantum yields (PLQYs) were measured utilizing a QE 2000 quantum efficiency measurement system (Otsuka Electronics).

Quantum chemical calculation. The calculations were performed using the Gaussian 09 E01 package.¹ The ground state geometries were optimized in B3LYP(D3)/6-311G* level in gas phase according to density functional theory (DFT). Based on the optimized ground state geometries, time-dependence density functional theory (TD-DFT) calculations were conducted in M062x/def2-TZVP level to study the excited state characters.²⁻⁵ The natural transition orbitals (NTOs) were analyzed using Multiwfn and visualized with VMD software.⁶⁻⁷ The calculated oscillator strengths were corrected by spin orbital coupling matrix element, which were calculated by ORCA in the same level of theory.⁸

2. Detailed results

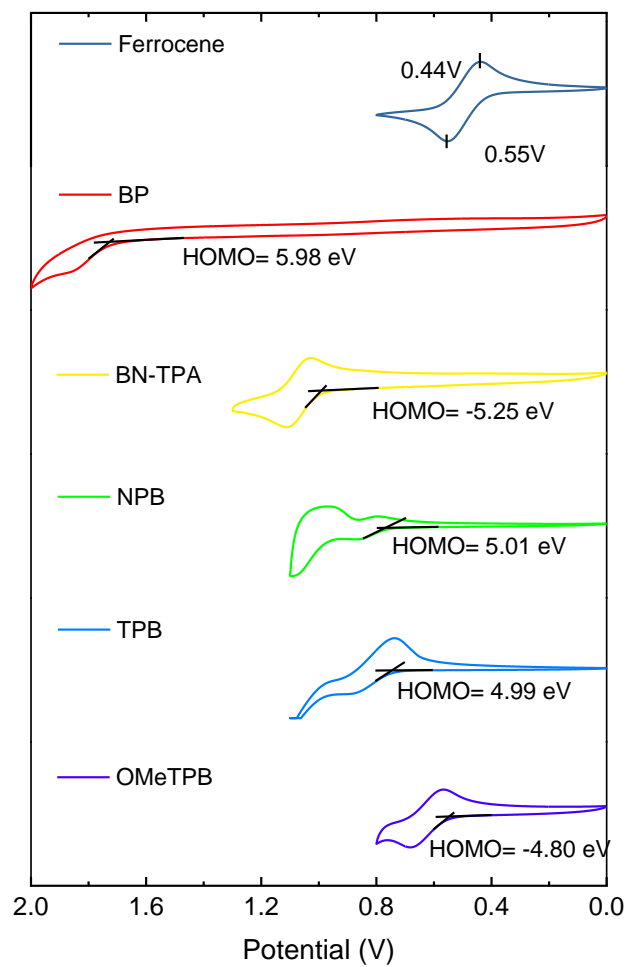


Figure S1. Cyclic voltammograms of the investigated compounds with 0.1 M $n\text{-Bu}_4\text{NPF}_6$ in $\text{CH}_2\text{Cl}_2/\text{acetonitrile}$ (4/1) solution using ferrocene as reference.

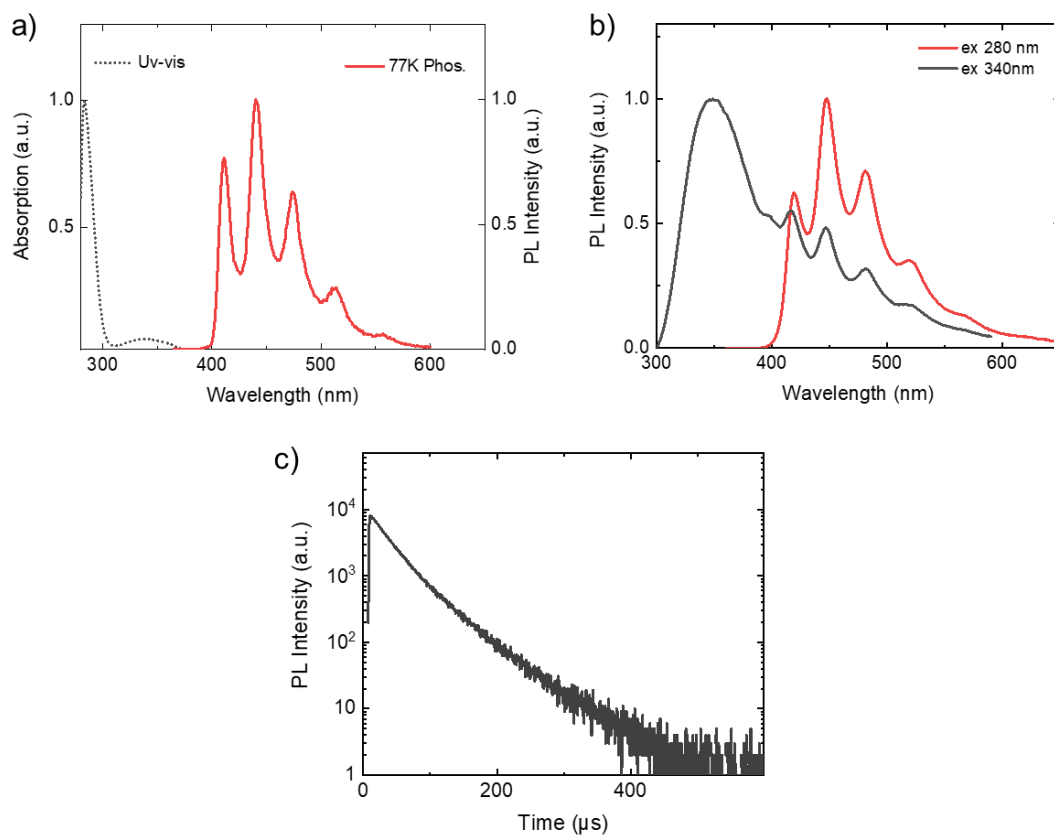


Figure S2. a) UV-vis absorption and phosphorescence spectra (measured at 77 K) of Benzophenone (BP) in toluene (concentration: 5×10^{-5} M); b) PL spectra of the BP solids measured at room temperature with different excitation wavelength, corresponding to the first peak ($n-\pi^*$ transition) and second peak ($\pi-\pi^*$ transient) in the absorption spectrum; c) Transient PL spectrum of the BP solids at RT excited at 360 nm.

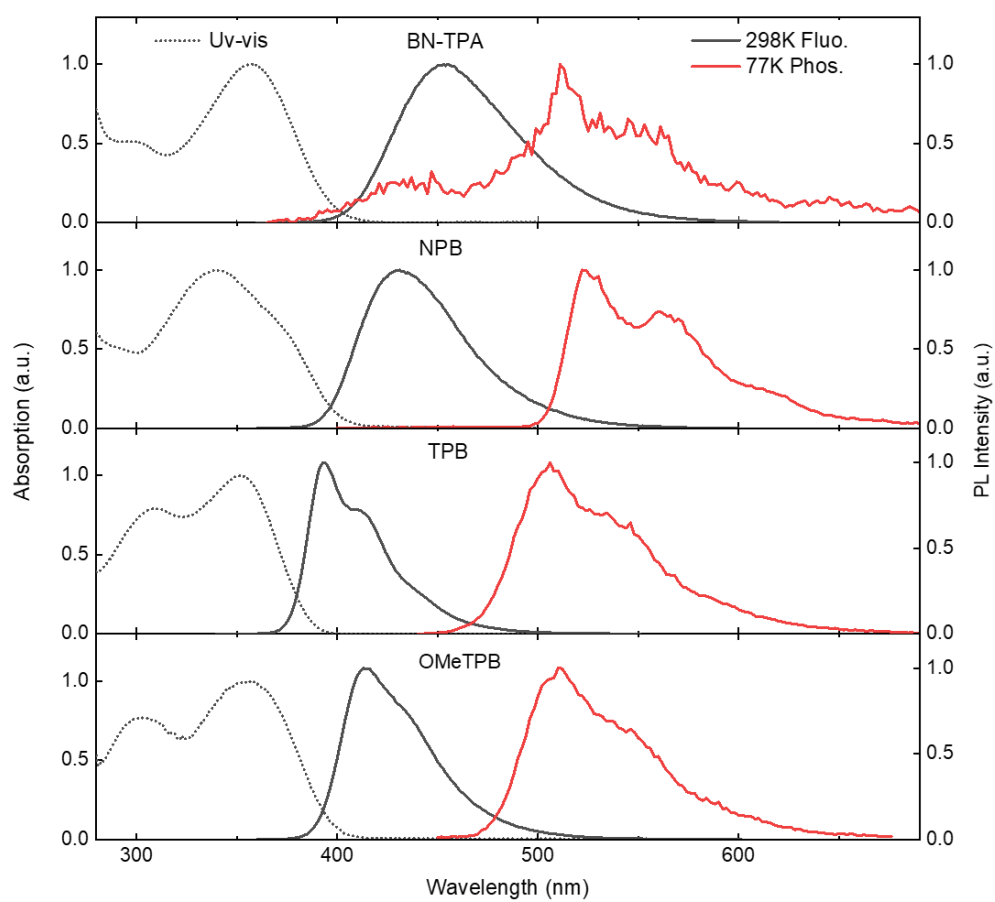


Figure S3. UV-vis absorption, fluorescence (measured at 298 K) and phosphorescence spectra (measured at 77 K) of the guest molecules in toluene (10^{-5} M).

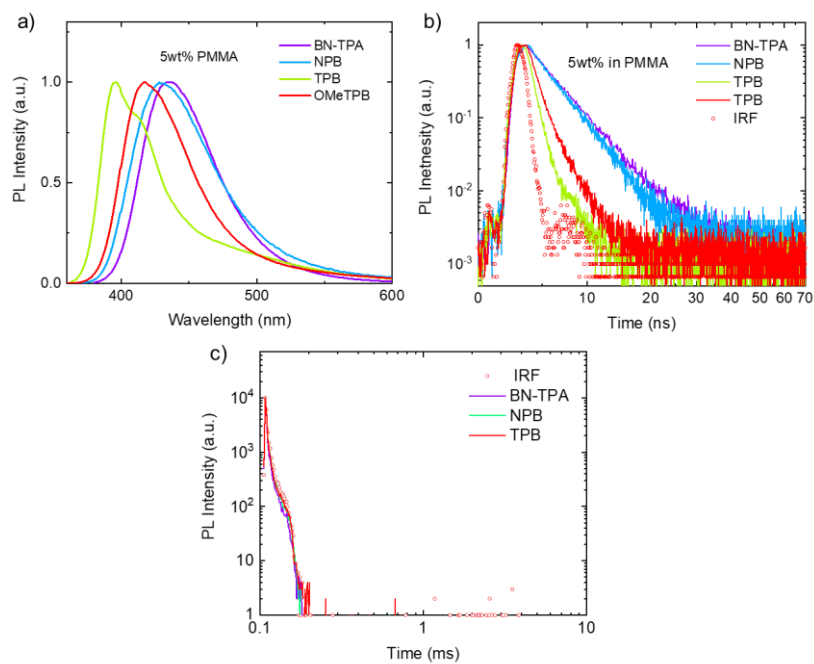


Figure S4. a) PL and b) transient PL decay character of the guest molecules in doped PMMA film (5wt%) in N_2 atmosphere; c) Transient PL decay character in 4ms time scale of the guest molecules doped in PMMA film (5wt%) measured in N_2 atmosphere at 530nm, and no long-lived delay component were detected.

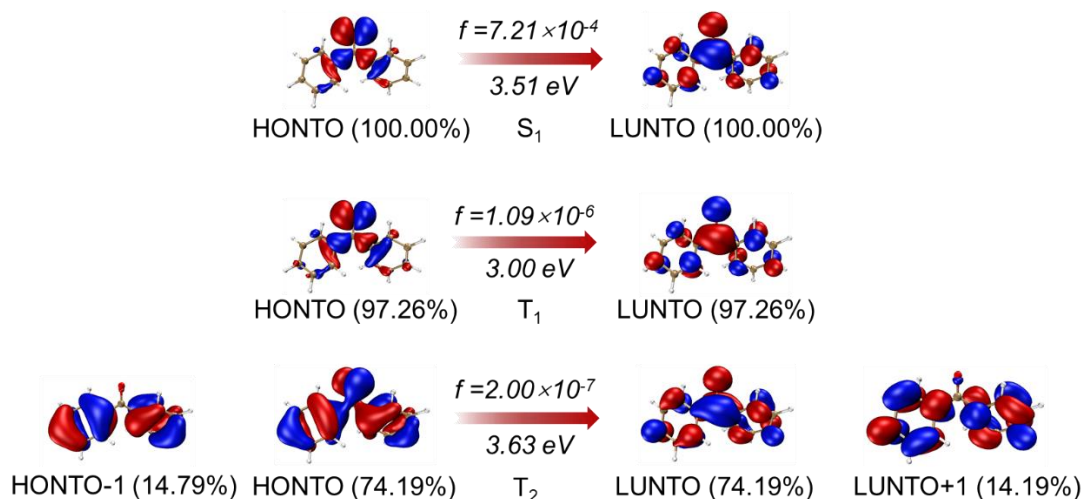


Figure S5. Natural Transition orbitals (NTO) distributions, corresponding eigenvalues, transition energy and oscillator strengths of BP, where HONTO, LUNTO, f denote highest occupied natural transition orbitals, lowest unoccupied natural transition orbital, oscillator strength respectively.

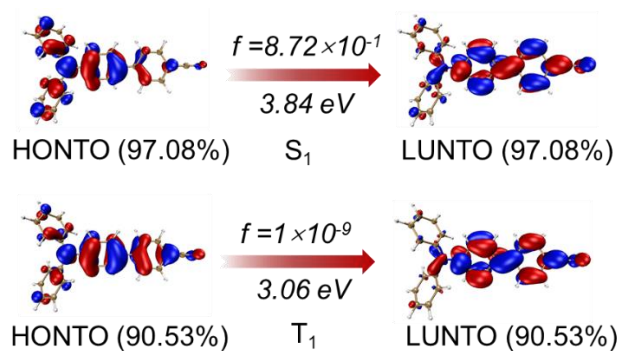


Figure S6. NTO distributions, corresponding eigenvalues, transition energy and oscillator strengths of BN-TPA.

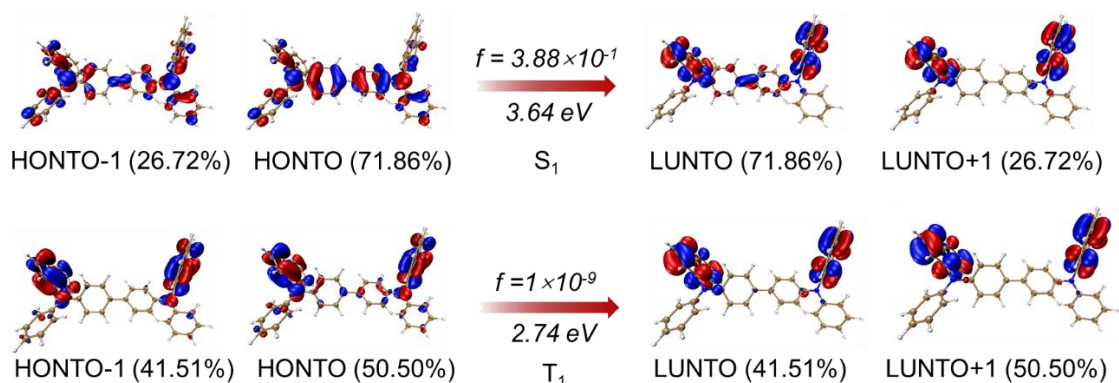


Figure S7. NTO distributions, corresponding eigenvalues, transition energy and oscillator strengths of NPB.

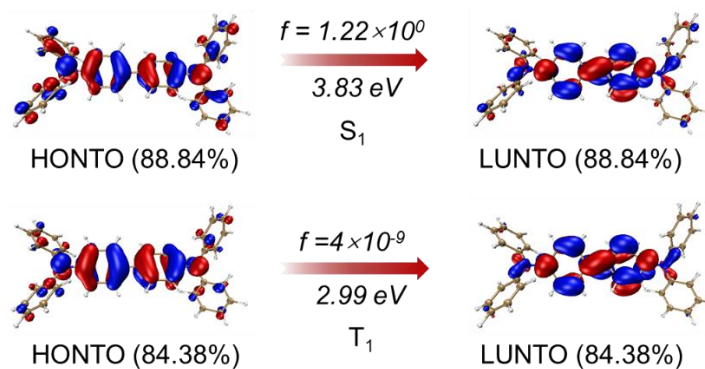


Figure S8. NTO distributions, corresponding eigenvalues, transition energy and oscillator strengths of TPB.

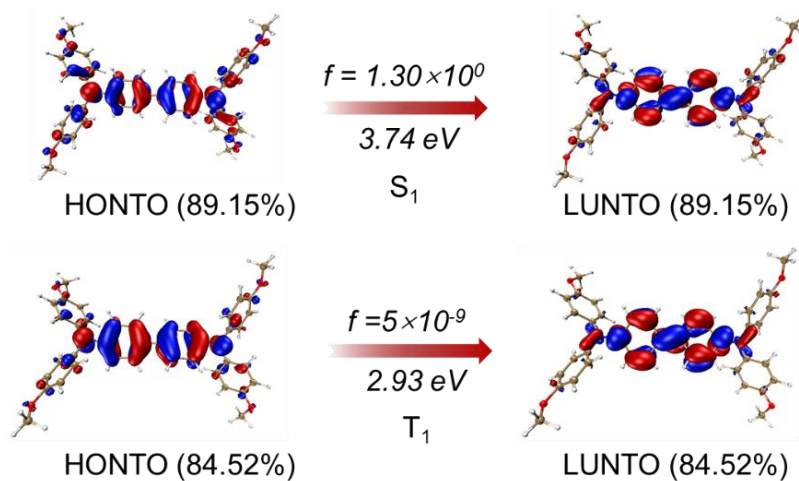


Figure S9. NTO distributions, corresponding eigenvalues, transition energy and oscillator strengths of OMeTPB.

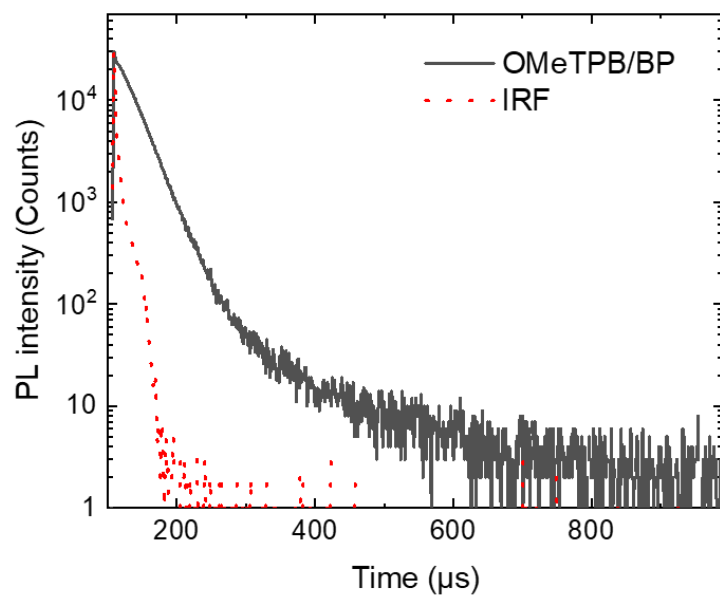


Figure S10. Transient PL decay character of the OMeTPB/BP system.

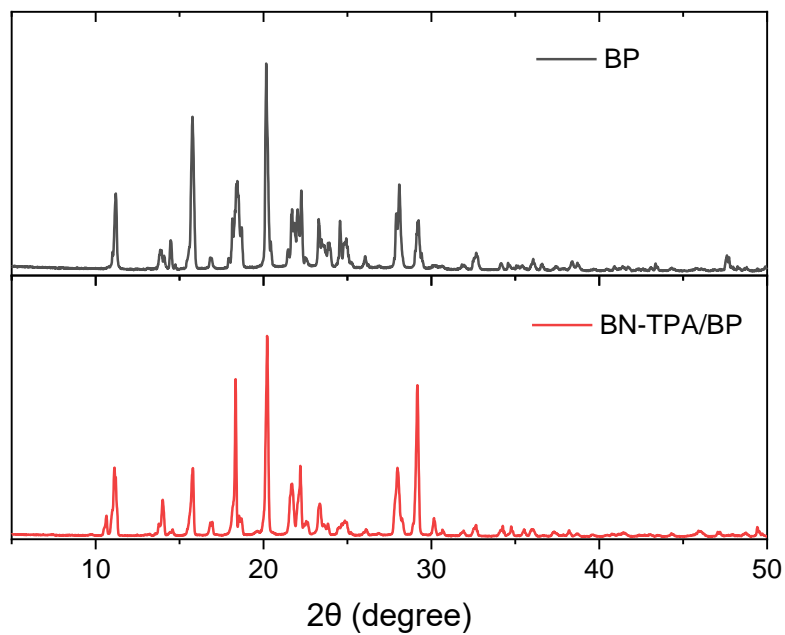


Figure S11. Powder X-ray diffraction patterns of the BP host and BN-TPA/BP doping system.

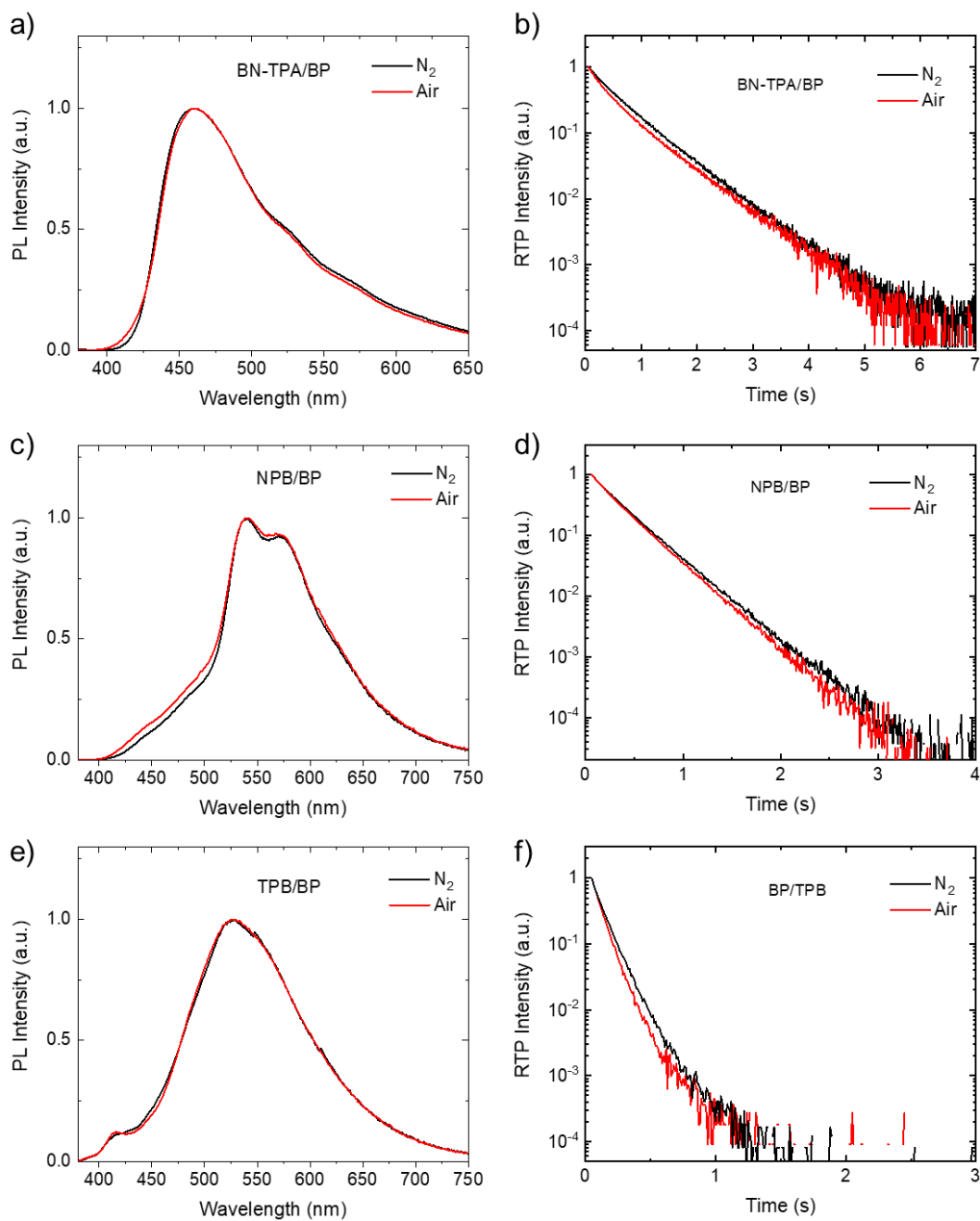


Figure S12. Steady state PL spectra and RTP decay characters of the binary systems in nitrogen atmosphere and air.

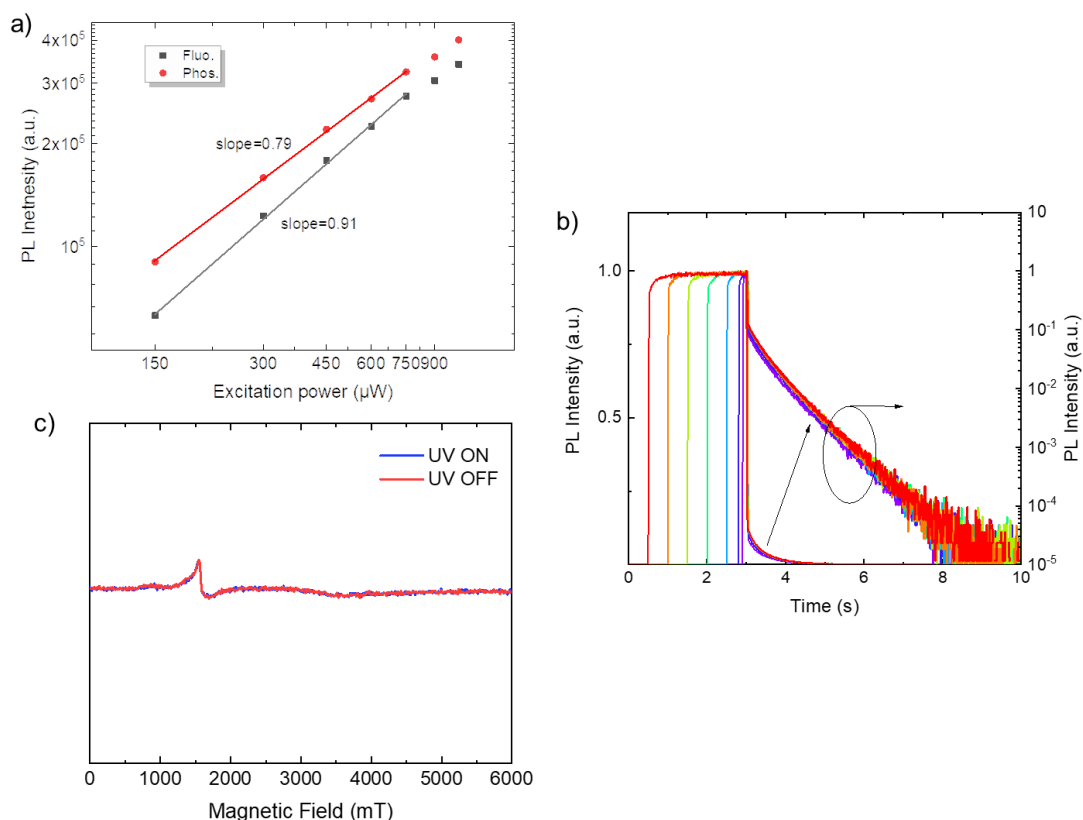


Figure S13. a) Excitation intensity dependent PL intensity of the fluorescence and phosphorescence peak in the BN-TPA/BP system; b) kinetic scanning of the phosphorescence intensity on the phosphorescence peak (550nm) in BN-TPA/BP with different excitation duration, the decay characters were plotted in logarithmic graph (right); c) electron spin resonance (ESR) spectra of BN-TPA/BP system in the present and absent of the 365 nm excitation light. The signal at 1500 mT was originated from the trace amount of Fe in the NMR tube for ESR measurement.

Different from the reported organic long persistent luminescence (OLPL) systems,⁹⁻¹¹ the donor-acceptor blending systems will not undergo charge separation and form OLPL, which is evidenced by the exponential decay character of phosphorescence and the absent of free radical absorption in the ESR spectra. This might due to the stronger binding energy in BN-TPA/BP binary system in compared with the reported exciplex systems. Moreover, the charge separation in OLPL systems is also mediated by the triplet CT state.¹² In these systems, the lowest triplet state is the triplet of the guest. The reverse electron transfer from CT state to the locally excited triplet state of the guest can reduce the population and lifetime of the intermediate CT state. Therefore, charge separation is less likely to happen and RTP emission from the guest is responsible for the long-lived emissions.

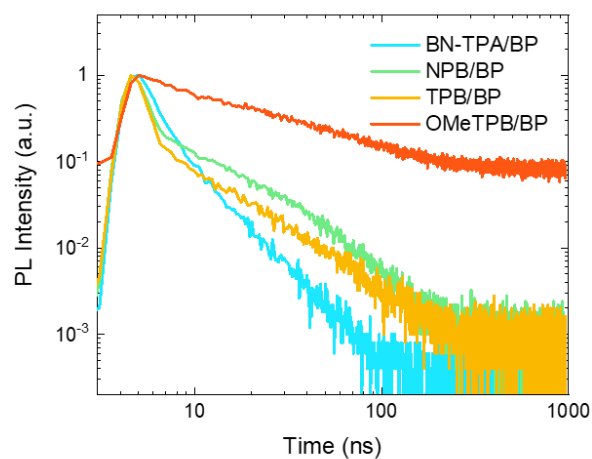


Figure S14. Transient PL of the host-guest systems in the fluorescence band in 1 μ s time range. The wavelength for measurement were selected according to the peak of the prompt component of the host-guest systems (450 nm for BN-TPA: BP, 460 nm for NPB: BP and TPB: BP systems and 580 nm for OMeTPB: BP system, excited with a 371 nm plus laser).

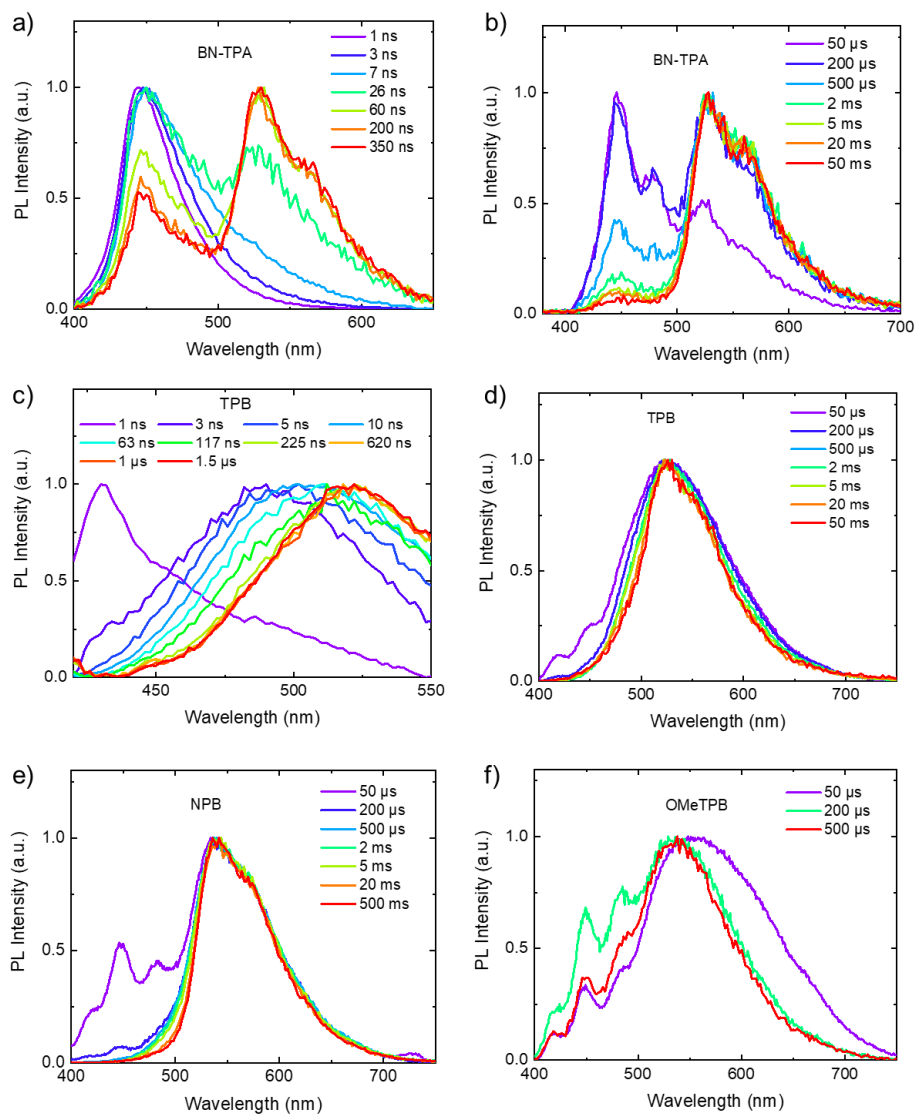


Figure S15. Time-resolved emission spectra and gated phosphorescence spectra with different gated time of the a), b) BN-TPA/BP and c), d) TPB/BP systems in the short time range; gated phosphorescence spectra of the e) NPB/BP and f) OMeTPB/BP systems.

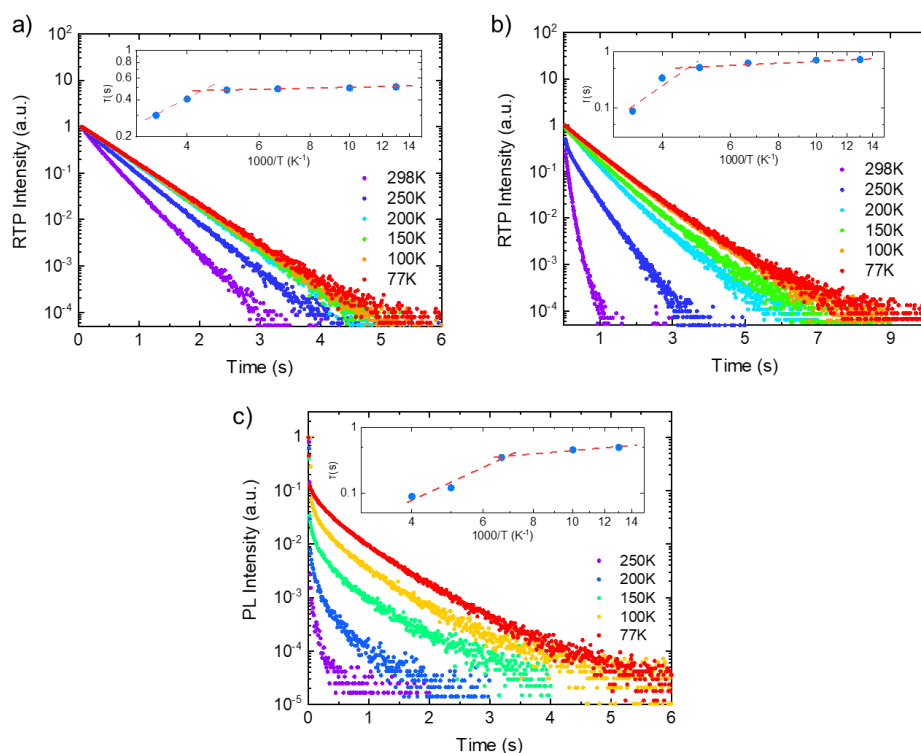


Figure S16. Temperature dependent RTP decay character of the a) NPB/BP and b) TPB/BP and c) OMeTPB/BP systems and the insert graphs show the phosphorescence lifetime plotted as a function of $1000/T$ temperature.

The nonradiative deactivation of the triplet excitons contains two independent processes: exciton quenching and nonradiative transition. And they will have different temperature-dependent character, as shown in Figure 4 and Figure S16. The non-radiative transition depends on the electronic properties of the molecules, including spin-orbital coupling (SOC) and molecular vibrations. The SOC of the aromatic materials are usually small because of the absence of heavy atoms, evidenced by the small calculated oscillator strength of T_1 transition (considering the SOC effect). Moreover, they were embedded in the same BP crystalline matrix, where molecular motions are suppressed. Accordingly, the nonradiative transition of the guest molecules should be small, which cannot explain the notable difference in phosphorescent lifetimes. Generally, according to the previous research, triplet exciton quenching process in host-guest systems is influenced by: energy transfer from guest to host, exciton diffusion, concentration quenching and quenching caused by oxygen.¹³⁻¹⁴ However, in these systems, the above-mentioned factors should be similar because the guest molecules are in the same host matrix and they have similar triplet energies. And exciton quenching from host is less likely to happen in host-guest system with a large triplet energy difference. Thus, the quenching by the intermediate CT state is the main triplet nonradiative deactivation channel at RT.

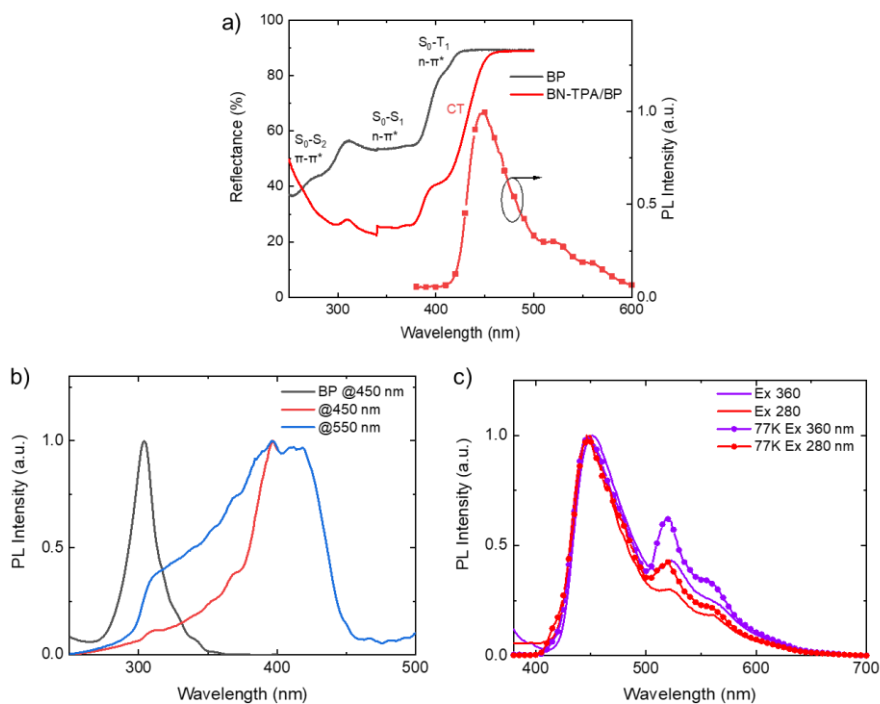


Figure S17. a) Solid state reflection spectra of BP and BN-TPA/BP (left) and PL spectra of BN-TPA. Enhanced absorption is noted in the BN-TPA/BP at long wavelength, indicating the formation of host-guest charge transfer state. b) Excitation spectra of BP and BN-TPA/BP system; c) PL spectra of the BN-TPA/BP excited at 360 nm and 280 nm at RT and 77K, respectively.

Given that the host BP with a $n-\pi^*$ transition character shows a short phosphorescence dominated emission, the population of guest triplet by sensitization i.e. Dexter energy transfer cannot be excluded.¹⁵⁻¹⁶ And sensitization methods have been proposed to detect the phosphorescence of the fluorophores in solution.¹⁷⁻¹⁸ However, this process is not efficient considering a large triplet-triplet energy gap between host and guest (less spectra overlap) and the low doping concentration. Moreover, the phosphorescence of BP can barely be excited with excitation wavelength larger than 360 nm because of the forbidden $n-\pi^*$ transition (Figure S16). For comparison, the excitation spectra of BN-TPA/BP indicates that the strongest excitation wavelength of phosphorescence lies in its CT band (360-400 nm), which further implies the key role of the CT state. In addition, the relative intensity of phosphorescence excited with 360 nm light is larger than that excited with 280 nm (corresponding to $\pi-\pi^*$ transition of BP host). These results indicate that, in spite of the strong ISC in the host matrix, host-guest Dexter energy transfer contributes little to the population of guest triplet and the formation of intermolecular charge transfer state plays a majority role in obtaining RTP in the host-guest systems.

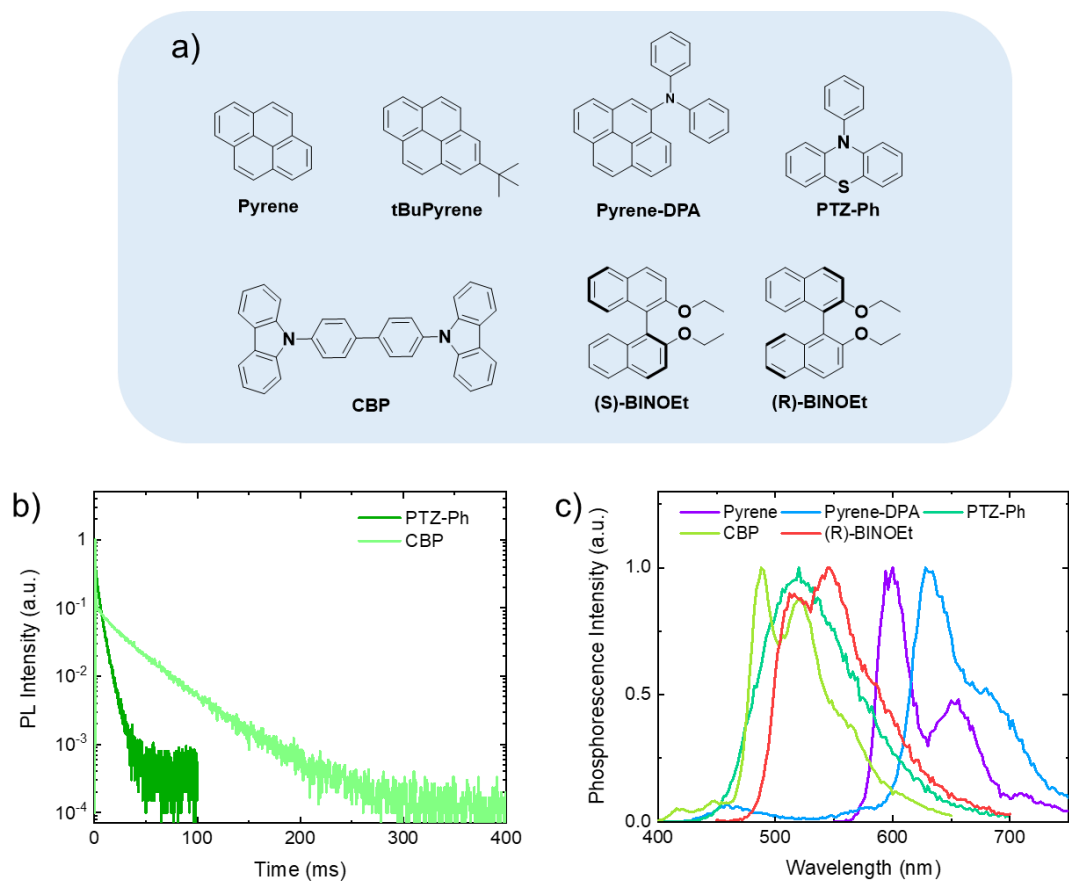


Figure S18. a) Molecule structures of the investigated guests; b) transient PL of the PTZ-Ph/BP and CBP/BP systems; c) Phosphorescence spectra of the host guest systems (delay 5 ms).

The abbreviations of the guest molecules denote:

tBuPyrene: 2-(tert-butyl) pyrene

Pyrene-DPA: N, N-diphenylpyren-4-amine

PTZ-Ph: 10-phenyl-10H-phenothiazine

CBP: 4,4'-di(9H-carbazol-9-yl)-1,1'-biphenyl

(S)-BINOEt: (S)-2,2'-diethoxy-1,1'-binaphthalene

(R)-BINOEt: (R)-2,2'-diethoxy-1,1'-binaphthalene

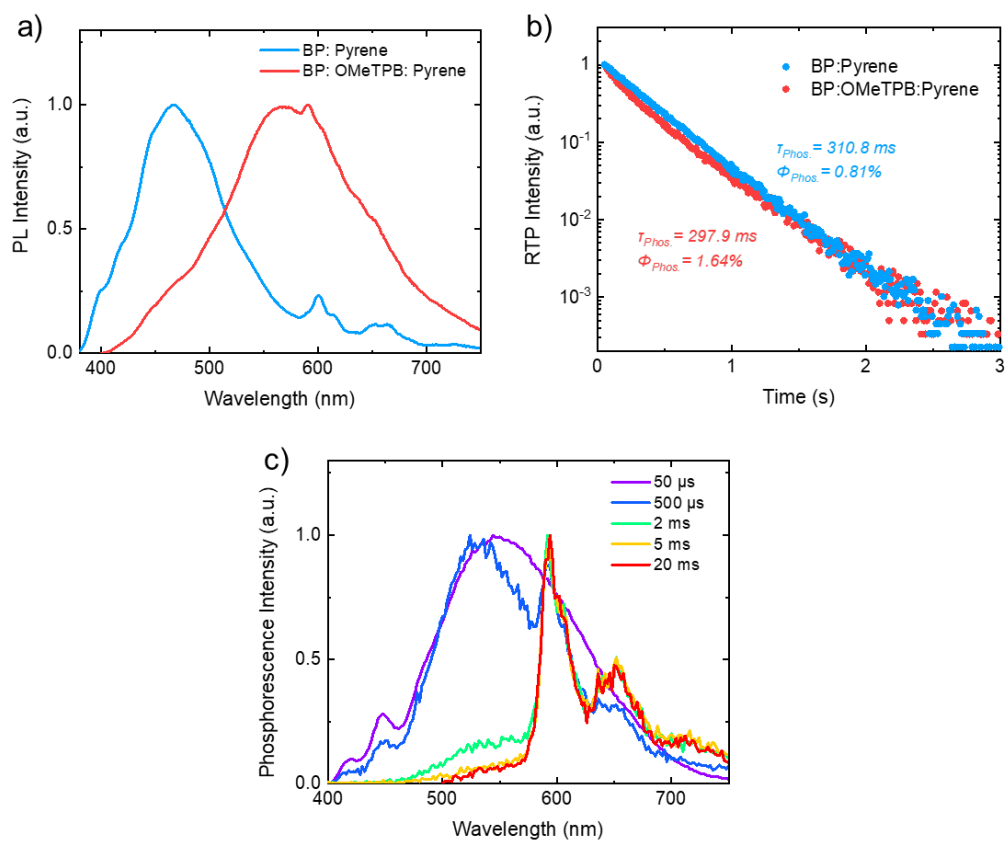


Figure S19. a) PL, b) RTP decay character of the BP/OMeTPB/Pyrene (mass ratio: 99: 1: 1) ternary system in compared with the Pyrene/BP binary system and c) phosphorescence spectra with different delay times in the BP/OMeTPB/Pyrene ternary system.

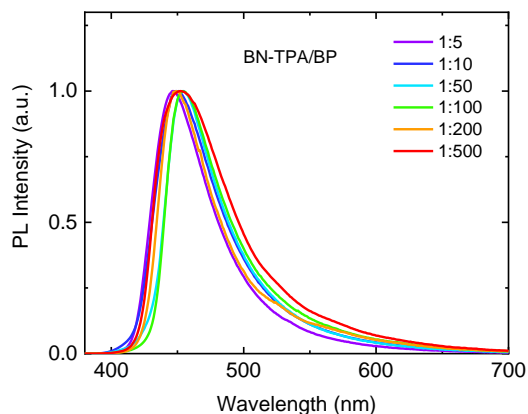


Figure S20. Steady state PL spectra of the BN-TPA/BP systems with different doping concentration.

The samples of BN-TPA/BP with different guest-host mass ratio from 1:5 to 1:500 were fabricated to investigate the effect of doping concentration on phosphorescence and the formation of the CT states. According to the steady state PL spectra, the prompt emission gradually red-shifts and then blue-shifts as the doping concentration decreases. The red-shifted emission can be attributed to the solvatochromism effect of the charge transfer states because more host-guest charge transfer states can be formed with increasing host ratio. And then, with excessive host ratio, the host can serve as diluents to reduce the interactions of the charge transfer states, which leads to the blueshifted emission. The effect of doping concentration on phosphorescence emission is inapparent, with similar relative intensity compared with the prompt emission peak.

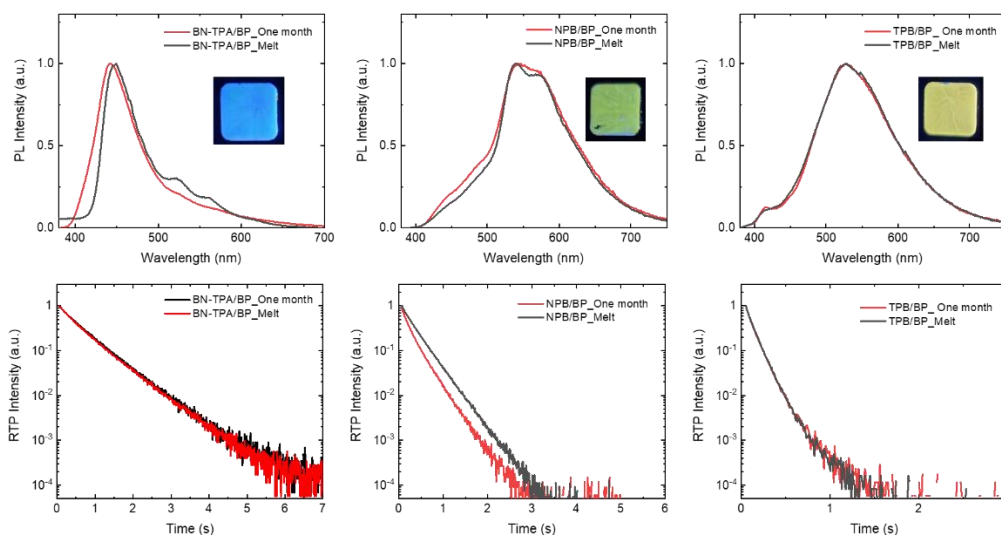


Figure S21. Comparison of the Steady state PL spectra and phosphorescence decay characters between the fresh sample and the sample placed in air for a month, the insert graphs show the sample excited by a 365nm LED.

3. Calculation of the exciton dynamic rate constants

The decay rate of fluorescence depends on the rates of fluorescence ($k_{Fluo.}$), nonradiative transition (k_{nr}^S), intersystem crossing (k_{ISC}) and electron transfer between host and guest (k_{et}):

$$\tau_{Fluo.} = \frac{1}{k_{Fluo.} + k_{nr}^S + k_{ISC}}$$

$$\tau'_{Fluo.} = \frac{1}{k_{Fluo.} + k_{nr}^S + k_{ISC} + k_{et}}$$

Assuming a constant $k_{Fluo.}$, k_{nr}^S and k_{ISC} of the guest in different matrix, the rate constant for charge transfer can be determined by:

$$k_{et} = \frac{1}{\tau'_{Fluo.}} - \frac{1}{\tau_{Fluo.}}$$

The deactivation process of the triplet excitons including phosphorescence emission, nonradiative transition (molecular vibration relaxation) and exciton quenching, thus the phosphorescent lifetime $\tau_{Phos.}$ can be expressed as:

$$\tau_{Phos.} = \frac{1}{k_{Phos.} + k_{nr} + k_q}$$

Where $k_{Phos.}$, k_{nr} , k_q stand for rate constants of radiative, nonradiative transition and exciton quenching of triplet excitons. According to the temperature-dependent RTP decay characters, the phosphorescent lifetime changes a little at low temperature (77K and 100K). This indicates that the non-radiative transition and exciton quenching are suppressed at low temperature. Given that exciton quenching is the dominated process at room temperature and the deactivation processed of the triplet excitons are suppressed at 77K, the rate constant for nonradiative transition and exciton quenching at room temperature can be determined by the change in phosphorescent lifetime at RT ($\tau_{p,RT}$) and 77K ($\tau_{p,77K}$):

$$k_{nr} + k_q = \frac{1}{\tau_{p,RT}} - \frac{1}{\tau_{p,77K}}$$

And the rate constant of phosphorescence emission can be expressed as:

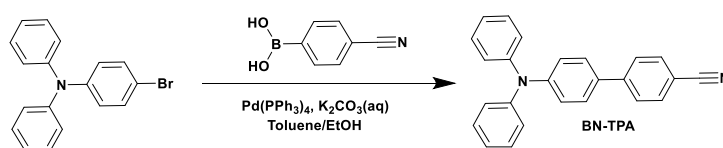
$$k_{Phos.} = \frac{1}{\tau_{Phos.}} - (k_{nr} + k_q)$$

τ_{Delay} and Φ_{Delay} in table 1 denotes phosphorescent lifetime and quantum yield for BN-TPA: BP, NPB: BP and TPB: BP systems and lifetime and percentage of the delayed component in the OMeTPB: BP system. Phosphorescent quantum yield was calculated according to total photoluminescence quantum yield and the phosphorescence intensity in steady state PL spectrum by multiple peaks gaussian function fitting. While the percentage and lifetime of the delayed component of the OMeTPB: BP system was calculated according to the fitted data in the transient PL spectrum.

4. Materials

4,4'-di(9H-carbazol-9-yl)-1,1'-biphenyl (CBP) and N^4,N^4 -di(naphthalen-1-yl)- N^4,N^4 -diphenyl-[1,1'-biphenyl]-4,4'-diamine (NPB) were purchased from Lumtec. and used without further purification. Benzophenone was obtained from Aladdin (purified by vacuum sublimation). N^4,N^4,N^4,N^4 -tetraphenyl-[1,1'-biphenyl]-4,4'-diamine (TPB), N^4,N^4,N^4,N^4 -tetrakis(4-methoxyphenyl)-[1,1'-biphenyl]-4,4'-diamine (OMeTPB), pyrene and 10-phenyl-10H-phenothiazine (PTZ-Ph) were obtained from TCI Chemicals and Energy Chemicals and further purified by recrystallization. All solvents and reagents were used as received from commercial suppliers without any further purification. All final products were purified by vacuum sublimation.

Synthesis of 4'-(diphenylamino)-[1,1'-biphenyl]-4-carbonitrile (BN-TPA):



Scheme 1. Synthesis of BN-TPA.

4-Bromo-N,N-diphenylaniline (1.3 g, 4 mmol), (4-cyanophenyl)boronic acid (705 mg, 4.8 mmol), K₂CO₃ (2 M in H₂O, 40 mL), toluene (120 mL) and ethanol (50 mL) were added into a 250 mL three-necked flask under Argon atmosphere. After stirring vigorously at room temperature for 20 min, tetrakis(triphenyl-phosphine) palladium(0) (Pd(PPh₃)₄) (231.2 mg, 0.2 mmol) was added into the solution. The mixture was heated to 100 °C and refluxed for 4 hours. The solvent was removed under reduced pressure and reaction mixture was then extracted with dichloromethane (DCM), washed by deionized water and brine solutions. The residues were further purified by column chromatography (eluent: petroleum ether/dichloromethane= 4/1) to afford white solids (1.29 g, 93%) ¹H NMR (400 MHz, Chloroform-d) δ 7.67 (q, J = 8.3 Hz, 4H), 7.50 – 7.42 (m, 2H), 7.30 (t, J = 7.8 Hz, 4H), 7.14 (dd, J = 8.4, 3.0 Hz, 6H), 7.08 (t, J = 7.3 Hz, 2H). ¹³C NMR (101 MHz, CDCl₃) δ 148.59, 147.28, 145.08, 132.61, 129.45, 127.89, 126.96, 124.96, 123.60, 123.04, 119.16, 110.09. APCI-MS (mass m/z): Calc. (C₂₅H₁₈N₂): 346.43, Found 346.6.

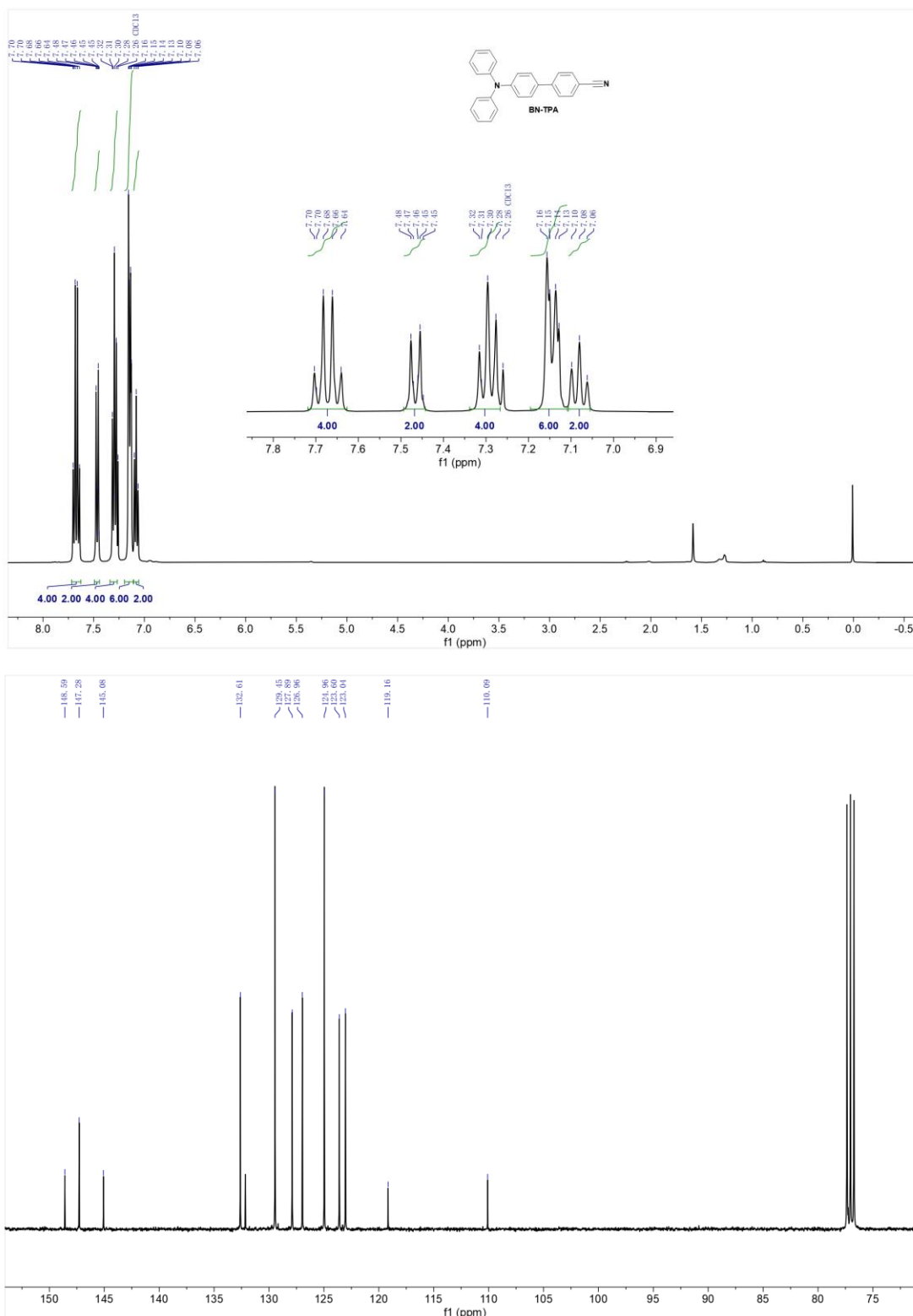
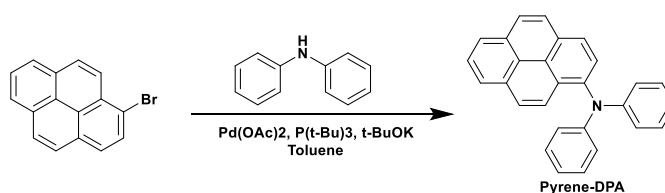


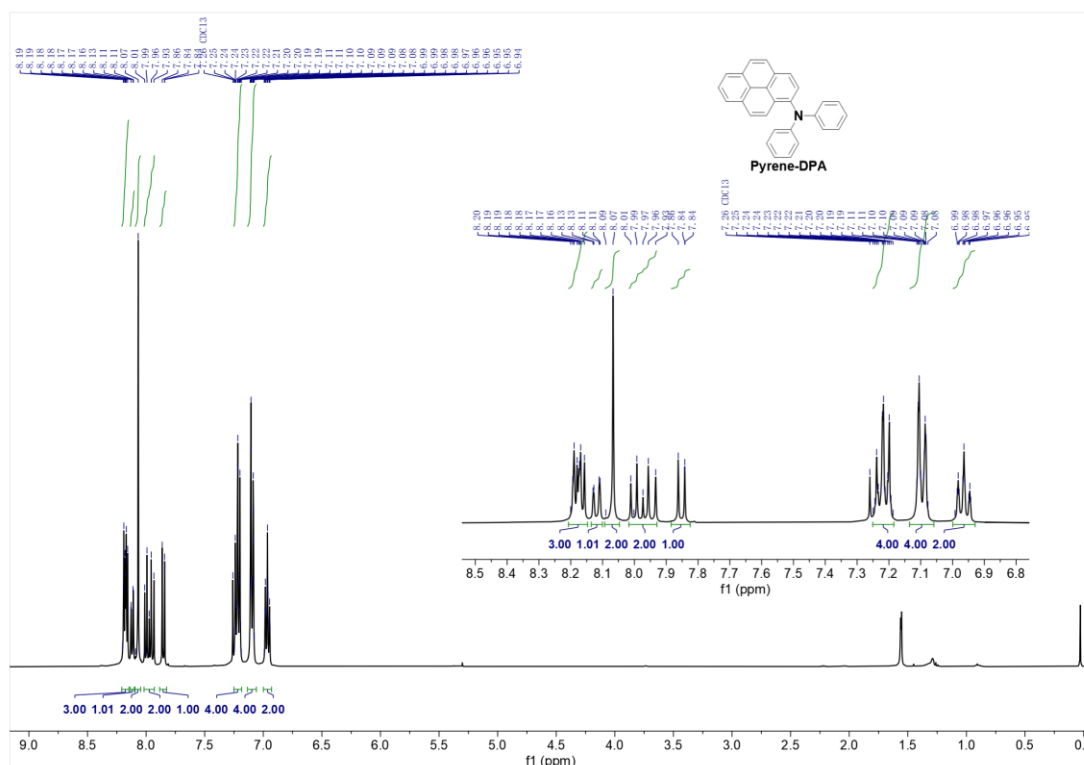
Figure S22. ^1H and ^{13}C NMR spectra of BN-TPA.

Synthesis of *N,N*-diphenylpyren-1-amine (Pyrene-DPA):



Scheme 2. Synthesis of Pyrene-DPA.

1-Bromopyrene (1.12 g, 4 mmol), diphenylamine (710.8 mg, 4.2 mmol), and potassium *t*-butoxide (771.2 mg, 8 mmol) were added into a 100 mL three neck flask with 50 ml toluene in Argon atmosphere. After degassing for 15 min, acetic acid palladium (II) ($\text{Pd}(\text{OAc})_2$) (45 mg, 0.2 mmol) and tri-*tert*-butylphosphine (1 mL, 1 M in toluene) were added. Subsequently, the mixture was stirred and refluxed overnight. After removing the solvent in reduced pressure, the mixture was partitioned between DCM and water. The combined organic layers were washed with brine, dried over anhydrous Mg_2SO_4 and concentrated in vacuo. The residues were further purified by column chromatography (eluent: petroleum ether/dichloromethane= 3/1) to afford yellow solids (1.11 g, 75%). ^1H NMR (400 MHz, Chloroform- d) δ 8.21 – 8.15 (m, 3H), 8.12 (dd, J = 7.7, 1.2 Hz, 1H), 8.07 (s, 2H), 8.02 – 7.93 (m, 2H), 7.85 (d, J = 8.2 Hz, 1H), 7.25 – 7.19 (m, 4H), 7.13 – 7.06 (m, 4H), 7.00 – 6.93 (m, 2H). ^{13}C NMR (101 MHz, CDCl_3) δ 148.71, 140.95, 131.28, 131.09, 129.58, 129.20, 128.24, 127.93, 127.71, 127.24, 127.13, 126.39, 126.23, 126.03, 125.22, 125.12, 124.87, 123.37, 122.12, 121.79. APCI-MS (mass m/z): Calc. ($\text{C}_{28}\text{H}_{19}\text{N}_1$): 369.47, found 370.3.



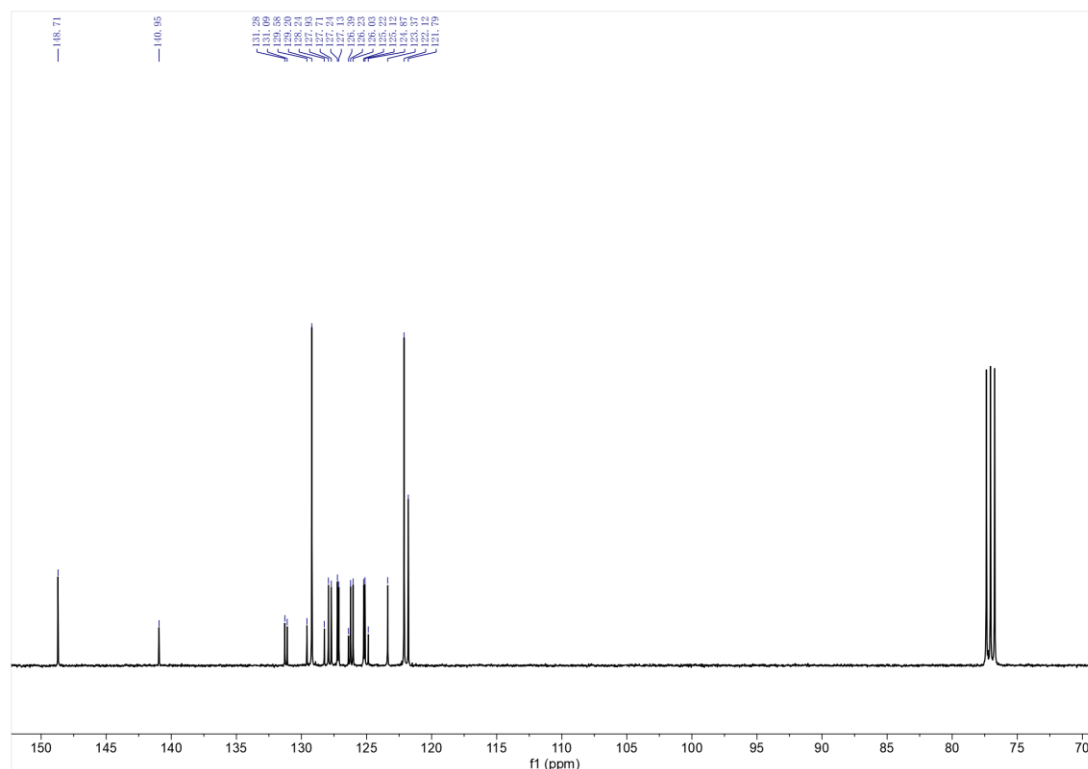
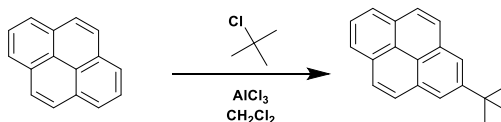


Figure S23. ^1H and ^{13}C NMR spectra of Pyrene-DPA.

Synthesis of 2-(tert-butyl) pyrene (tBuPyrene):



Scheme 3. Synthesis of tBuPyrene.

Pyrene (2 g, 10 mmol) and 2-chloro-2-methylpropane (3.23 mL, 30 mmol) were added into a 250mL three neck flask with 50 ml CH_2Cl_2 in Argon atmosphere. After cooling down to 0°C , anhydrous AlCl_3 (2.67 g, 20 mmol) was added in portion to the system. The mixture was stirred for 3h at room temperature and quenched with ice water. The combined organic layers were extracted with dichloromethane, washed with brine, dried over anhydrous Mg_2SO_4 and concentrated in vacuo. The residues were further purified by column chromatography (eluent: petroleum ether) to afford white solids (1.68 g, 65%). ^1H NMR (500 MHz, Chloroform- d) δ 8.24 (s, 2H), 8.16 (d, $J = 7.6$ Hz, 2H), 8.07 (d, $J = 1.0$ Hz, 4H), 7.99 (d, $J = 7.5$ Hz, 1H), 1.61 (s, 9H). ^{13}C NMR (101 MHz, CDCl_3) δ 148.71, 140.95, 131.28, 131.09, 129.58, 129.20, 128.24, 127.93, 127.71, 127.24, 127.13, 126.39, 126.23, 126.03, 125.22, 125.12, 124.87, 123.37, 122.12, 121.79. APCI-MS (mass m/z): Calc. ($\text{C}_{20}\text{H}_{18}$): 258.36, found 258.5.

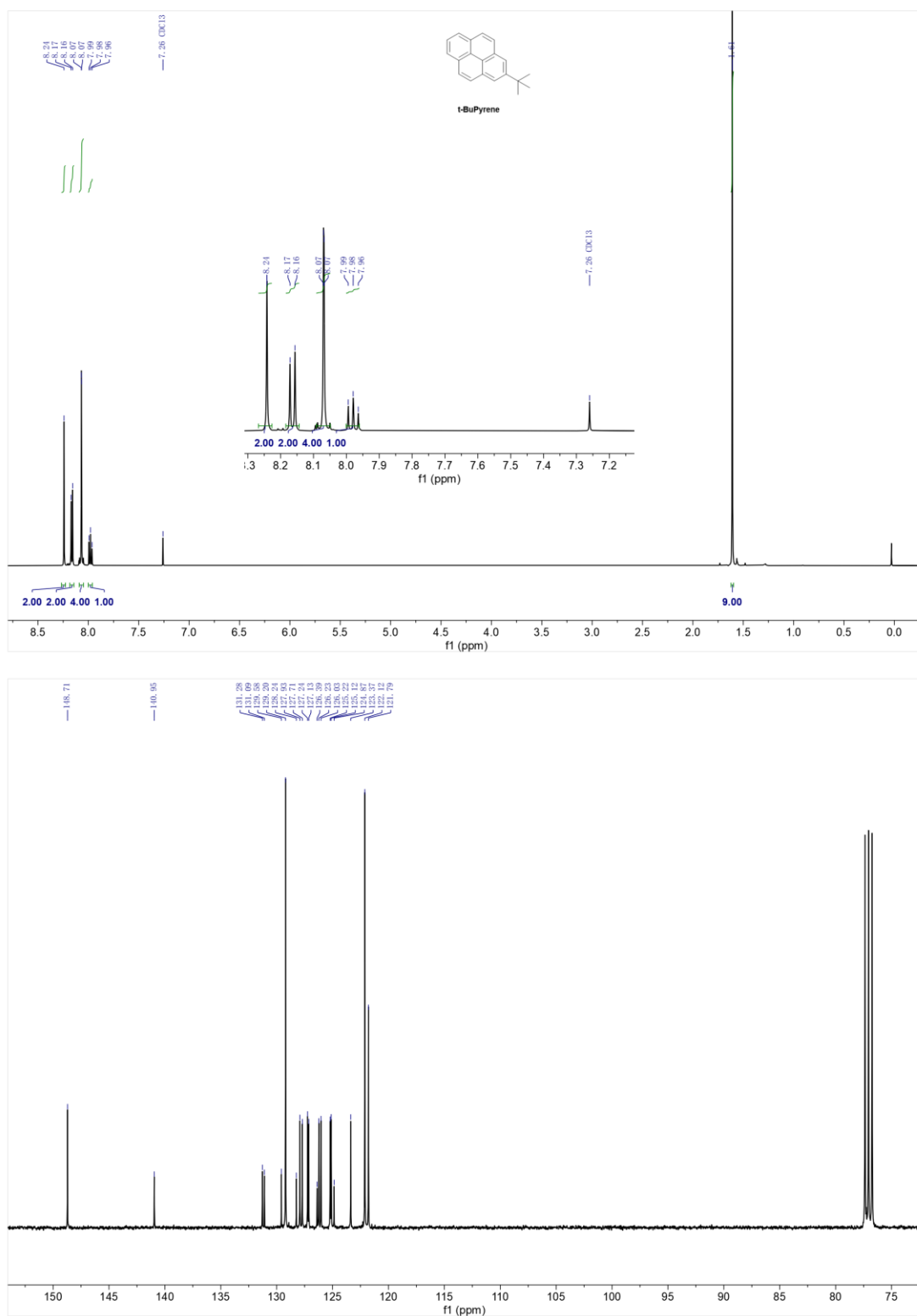
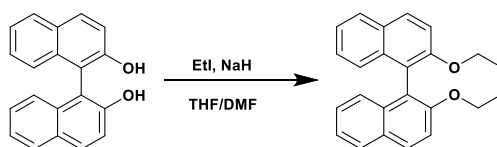


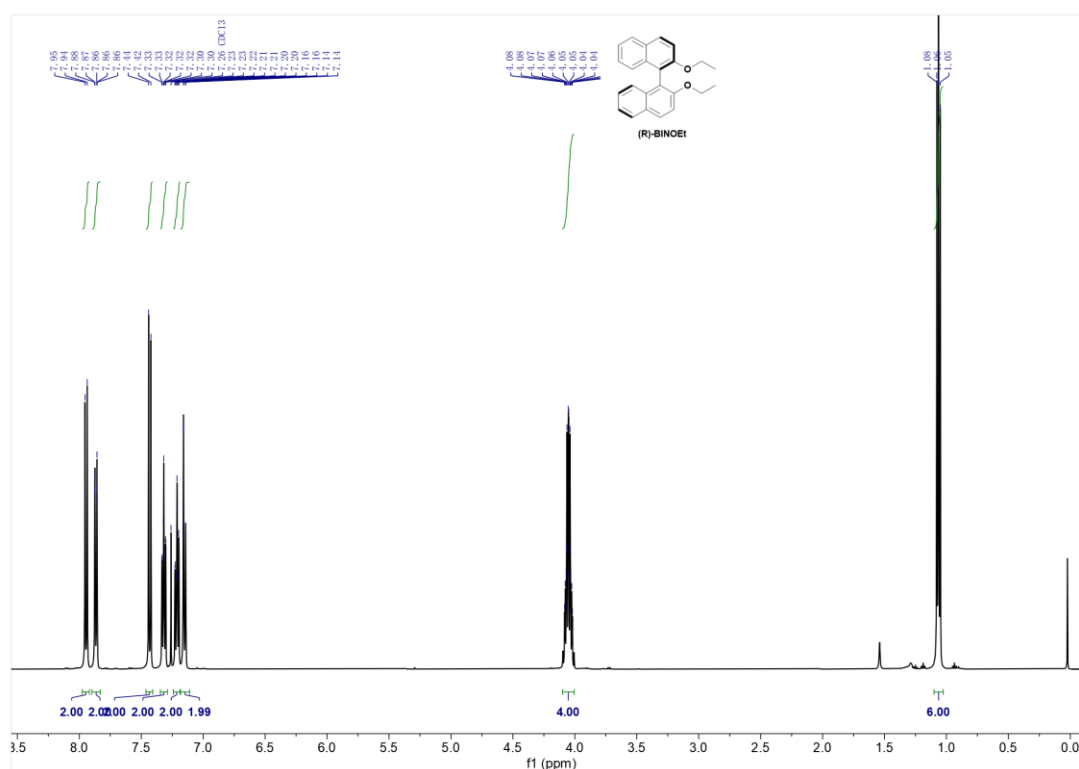
Figure S24. ^1H and ^{13}C NMR spectra of tBuPyrene.

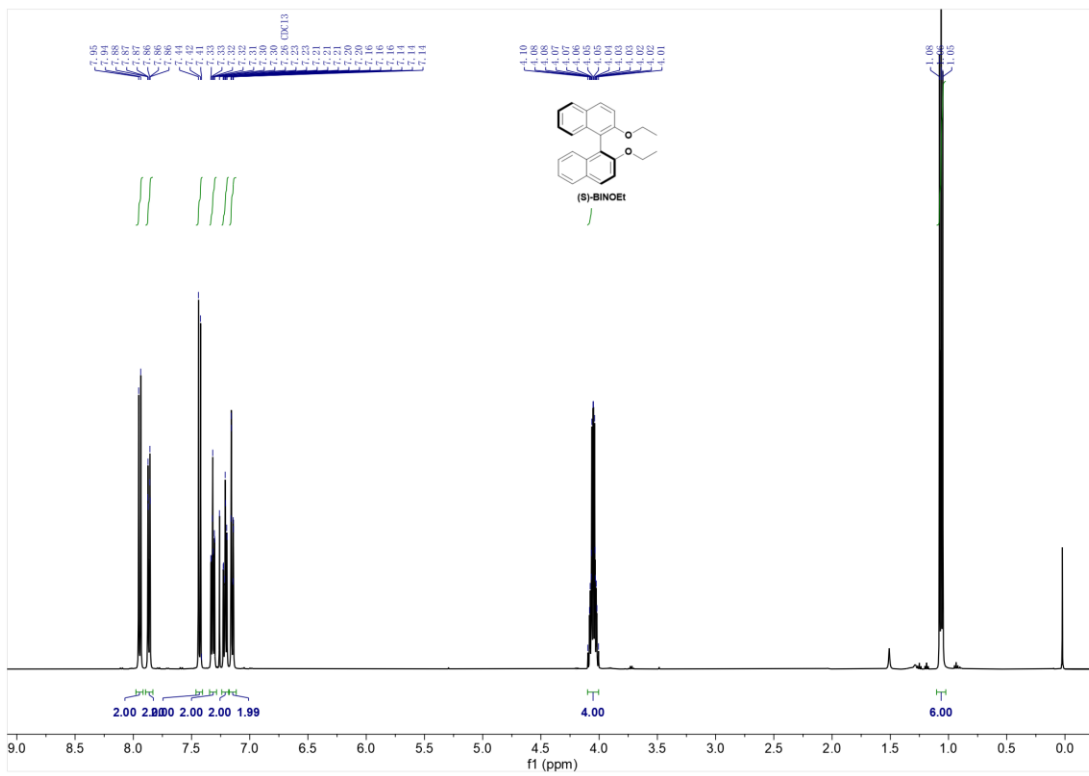
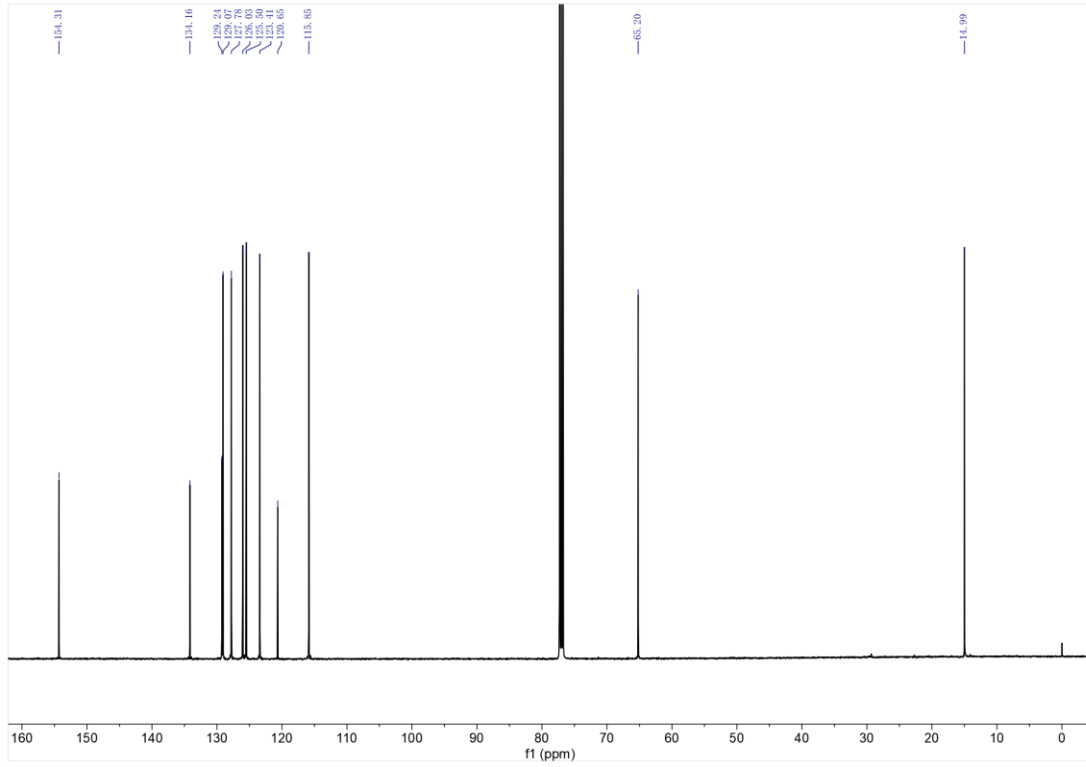
Synthesis of (R)-2,2'-diethoxy-1,1'-binaphthalene ((S)-2,2'-diethoxy-1,1'-binaphthalene):



Scheme 4. Synthesis of 2,2'-diethoxy-1,1'-binaphthalene.

(R)-[1,1'-binaphthalene]-2,2'-diol ((S)-[1,1'-binaphthalene]-2,2'-diol) (1.41 g, 5 mmol) was dissolved in THF/DMF mixed solution (5:2, 56 mL) in Argon atmosphere and Sodium hydride (600 mg, 60% in mineral oil, 15 mmol). After cooling down to 0°C, ethyl iodide (1.95g, 12.5mmol) was added dropwise in a syringe. The system was stirred at room temperature overnight and quenched with water. The combined organic layers were extracted with dichloromethane, washed with brine, dried over anhydrous Mg₂SO₄ and concentrated in vacuo. The residues were further purified by column chromatography (eluent: petroleum ether) to afford white solids (1.25 g, 73%). ¹H NMR (500 MHz, Chloroform-d) δ 7.95 (d, J = 9.0 Hz, 2H), 7.90 – 7.83 (m, 2H), 7.43 (d, J = 9.0 Hz, 2H), 7.32 (ddd, J = 8.1, 6.6, 1.3 Hz, 2H), 7.21 (ddd, J = 8.0, 6.6, 1.3 Hz, 2H), 7.15 (dd, J = 8.5, 1.2 Hz, 2H), 4.05 (qd, J = 7.0, 5.2 Hz, 4H), 1.06 (t, J = 7.0 Hz, 6H). ¹³C NMR (126 MHz, CDCl₃) δ 154.31, 134.16, 129.24, 129.07, 127.78, 126.03, 125.50, 123.41, 120.65, 115.85, 65.20, 14.99. APCI-MS (mass m/z): Calc. (C₂₄H₂₂O₂): 342.44, found 342.4.





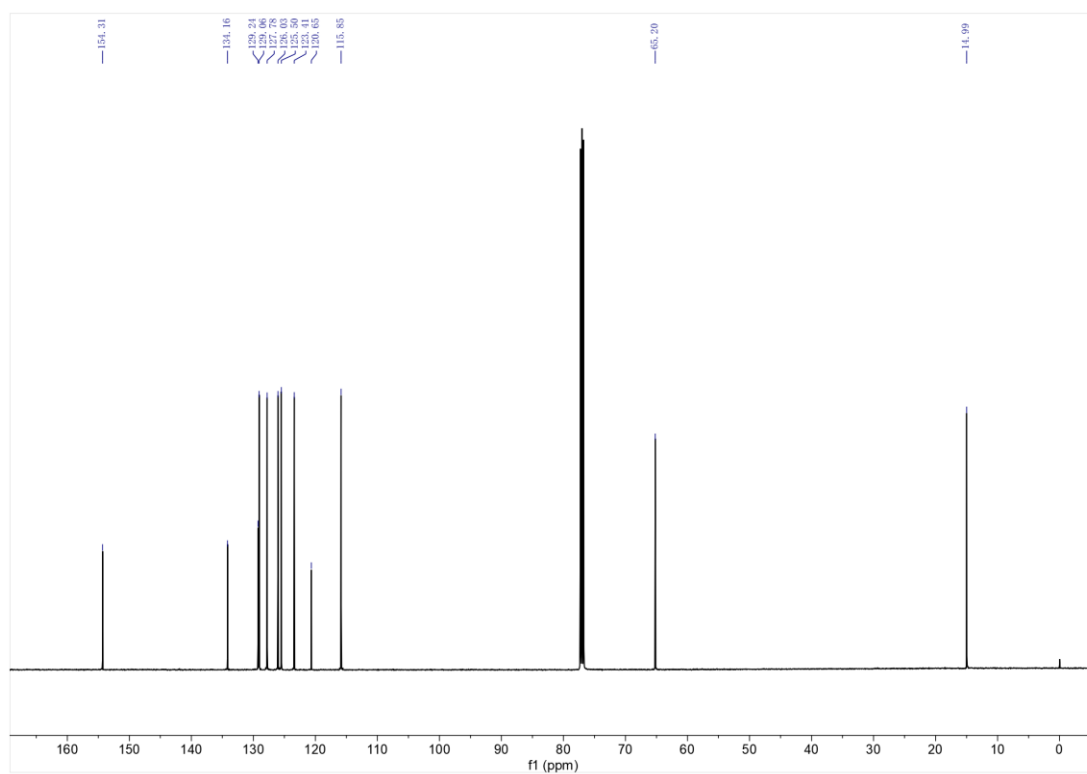


Figure S25. ^1H and ^{13}C NMR spectra of (R)-BINOEt and (S)-BINOEt.

References

1. Gaussian 09, R. A., M. J. Frisch, G. W. Trucks, H. B. Schlegel, G. E. Scuseria, M. A. Robb, J. R. Cheeseman, G. Scalmani, V. Barone, G. A. Petersson, H. Nakatsuji, X. Li, M. Caricato, A. Marenich, J. Bloino, B. G. Janesko, R. Gomperts, B. Mennucci, H. P. Hratchian, J. V. Ortiz, A. F. Izmaylov, J. L. Sonnenberg, D. Williams-Young, F. Ding, F. Lipparini, F. Egidi, J. Goings, B. Peng, A. Petrone, T. Henderson, D. Ranasinghe, V. G. Zakrzewski, J. Gao, N. Rega, G. Zheng, W. Liang, M. Hada, M. Ehara, K. Toyota, R. Fukuda, J. Hasegawa, M. Ishida, T. Nakajima, Y. Honda, O. Kitao, H. Nakai, T. Vreven, K. Throssell, J. A. Montgomery, Jr., J. E. Peralta, F. Ogliaro, M. Bearpark, J. J. Heyd, E. Brothers, K. N. Kudin, V. N. Staroverov, T. Keith, R. Kobayashi, J. Normand, K. Raghavachari, A. Rendell, J. C. Burant, S. S. Iyengar, J. Tomasi, M. Cossi, J. M. Millam, M. Klene, C. Adamo, R. Cammi, J. W. Ochterski, R. L. Martin, K. Morokuma, O. Farkas, J. B. Foresman, and D. J. Fox, Gaussian, Inc., Wallingford CT, 2016.
2. Runge, E.; Gross, E. K. U. Density-Functional Theory for Time-Dependent Systems. *Phys. Rev. Lett.* **1984**, *52* (12), 997-1000.
3. Dreuw, A.; Head-Gordon, M. Single-Reference ab Initio Methods for the Calculation of Excited States of Large Molecules. *Chem. Rev.* **2005**, *105* (11), 4009-4037.
4. Stephens, P. J.; Devlin, F. J.; Chabalowski, C. F.; Frisch, M. J. Ab Initio Calculation of Vibrational Absorption and Circular Dichroism Spectra Using Density Functional Force Fields. *J. Phys. Chem.* **1994**, *98* (45), 11623-11627.
5. Zhao, Y.; Truhlar, D. G. The M06 suite of density functionals for main group thermochemistry, thermochemical kinetics, noncovalent interactions, excited states, and transition elements: two new functionals and systematic testing of four M06-class functionals and 12 other functionals. *Theor. Chem. Acc.* **2008**, *120* (1), 215-241.
6. Lu, T.; Chen, F. Multiwfn: A multifunctional wavefunction analyzer. *J. Comput. Chem.* **2012**, *33* (5), 580-592.
7. Humphrey, W.; Dalke, A.; Schulten, K. VMD: visual molecular dynamics. *J. Mol. Graph.* **1996**, *14* (1), 33-8, 27-8.
8. Neese, F. The ORCA program system. *WIREs Computational Molecular Science* **2011**, *2* (1), 73-78.
9. Kabe, R.; Adachi, C. Organic long persistent luminescence. *Nature* **2017**, *550* (7676), 384-387.
10. Nishimura, N.; Lin, Z.; Jinnai, K.; Kabe, R.; Adachi, C. Many Exciplex Systems Exhibit Organic Long-Persistent Luminescence. *Adv. Funct. Mater.* **2020**, *30* (22), 2000795.
11. Lin, Z.; Kabe, R.; Wang, K.; Adachi, C. Influence of energy gap between charge-transfer and locally excited states on organic long persistence luminescence. *Nat Commun* **2020**, *11* (1), 191.
12. Xiao, L.; Wang, Z.; Zhang, C.; Xie, X.; Ma, H.; Peng, Q.; An, Z.; Wang, X.; Shuai, Z.; Xiao, M. Long Persistent Luminescence Enabled by Dissociation of Triplet Intermediate States in an Organic Guest/Host System. *J. Phys. Chem. Lett.* **2020**, *11* (9), 3582-3588.
13. Hirata, S. Recent Advances in Materials with Room-Temperature Phosphorescence: Photophysics for Triplet Exciton Stabilization. *Adv. Opt. Mater.* **2017**, *5* (17), 1700116.
14. Hirata, S.; Totani, K.; Zhang, J.; Yamashita, T.; Kaji, H.; Marder, S. R.; Watanabe, T.; Adachi, C. Efficient Persistent Room Temperature Phosphorescence in Organic Amorphous Materials under Ambient Conditions. *Adv. Funct. Mater.* **2013**, *23* (27), 3386-3397.
15. Totani, K.; Okada, Y.; Hirata, S.; Vacha, M.; Watanabe, T. Thermoresponsive Persistent

- Phosphorescent Color Change Using Efficient Thermally Activated Reverse Energy Transfer with a Large Energy Difference. *Adv. Opt. Mater.* **2013**, *1* (4), 283-288.
16. Spencer, T. S.; O'Donnell, C. M. Energy transfer in a hydrogen-bonded carbazole-benzophenone complex. *J. Am. Chem. Soc.* **1972**, *94* (14), 4846-4849.
17. Ermolaev, V. L. Energy Transfer in Organic Systems Involving the Triplet State iii. Rigid Solutions and Crystals. *Sov. Phys. Usp.* **1963**, *6* (3), 333-358.
18. Xu, Y.; Liang, X.; Zhou, X.; Yuan, P.; Zhou, J.; Wang, C.; Li, B.; Hu, D.; Qiao, X.; Jiang, X.; Liu, L.; Su, S. J.; Ma, D.; Ma, Y. Highly Efficient Blue Fluorescent OLEDs Based on Upper Level Triplet-Singlet Intersystem Crossing. *Adv. Mater.* **2019**, *31* (12), e1807388.